Optical Materials 105 (2020) 109897

Contents lists available at ScienceDirect

Optical Materials

journal homepage: http://www.elsevier.com/locate/optmat

# Performance optimization of $CH_3NH_3Pb(I_{1-x}Br_x)_3$ based perovskite solar cells by comparing different ETL materials through conduction band offset engineering

Ayyaz Ahmed [a], Kashif Riaz [a,**], Haris Mehmood [a], Tauseef Tauqeer [a], Zubair Ahmad [b,*]

[a] Department of Electrical Engineering, Information Technology University (ITU), 346-B, Ferozepur Road, Lahore, Pakistan
[b] Center for Advanced Materials (CAM), Qatar University, P. O. Box 2713, Doha, Qatar

ARTICLE INFO

*Keywords:*
Conduction band offset engineering
Perovskite solar cell
Electron transport layer
Hole transport layer
SCAPS
The power conversion efficiency

ABSTRACT

Numerical simulations can provide the physical insights into the carrier transport mechanism in the solar cells, and the factors influencing their performance. In this paper, perovskite solar cell (PSC) based on the mixed perovskite ($CH_3NH_3Pb(I_{1-x}Br_x)_3$ has been numerically simulated using the SCAPS simulator. A comparative analysis of different electron transport layers (ETLs) based on their conduction band offsets (CBO) has been performed, while Spiro-OMeTAD was used as a hole transport layer (HTL). Among the proposed ETLs, CdZnS performed better and demonstrated the power conversion efficiency (PCE) of 25.20%. Also, the PCE of the PSC has been optimized by adjusting the doping concentrations in the ETL, Spiro-OMeTAD layer, and the thickness of the perovskite light absorber layer. It was found that the doping concentration of $10^{21}$ $cm^{-3}$ for the CdZnS based ETL and $10^{20}$ $cm^{-3}$ for Spiro-OMeTAD are the optimum concentrations values for demonstrating enhanced efficiency. A 600 nm thick perovskite layer has found to be appropriate for the efficient PSC design. For the initial guessing and numerical model validation, the photovoltaic data of a very stable (over one year with PCE ~13%) n-i-p structured (ITO/$TiO_2$/$CH_3NH_3Pb(I_{1-x}Br_x)_3$/Spiro-OMeTAD/Au) PSCs was used. These numerically simulated results signify the optimum performance of the photovoltaic device that can be further implemented to develop the highly efficient PSCs.

## 1. Introduction

Perovskite solar cells (PSCs) have been recognized as an emerging candidate for future photovoltaic technology owing to their low cost, ease in fabrication, and high-power conversion efficiency (PCE). However, besides the stability issues and environmental factors, nonradiative recombination and losses are considered as the key factors to limit their performance [1–3]. Electron transport layer (ETL) and hole transport layer (HTL) are the major components of the PSCs, which can potentially reduce the nonradiative recombination and losses [4–8].

Specifically, ETL is an essential component of a PSC, which not only extracts the electrons from the perovskite absorber but also blocks the holes [9]. Since the development of dye-sensitized solar cells (DSSC), $TiO_2$ has been considered as a renowned ETL material due to its wide bandgap and chemical stability [10,11]. However, the deposition of $TiO_2$ based ETL requires high-temperature sintering (>450 °C), making it undesirable for large scale manufacturing and flexible PSCs [12]. Also, $TiO_2$ has low carrier mobility ($10^{-4}$ $cm^2$ $v^{-1}s^{-1}$) and low conductivity, causing poor charge transport in PSC [13]. Even though the doped $TiO_2$ layers have been used to improve the performance of the PSCs [14,15] but the stability is compromised due to doping. Also, Snaith et al. [16] reported that UV light activates charge traps and oxygen vacancies in $TiO_2$, which reduce the conversion efficiency of the PSCs due to the capturing of photogenerated carriers. There exists a conduction band offset (CBO) between $TiO_2$ and perovskite which results in interface recombination in PSCs [17]. Thus, due to above detrimental properties of $TiO_2$, it is crucial to explore new electron transport layer materials to further enhance the conversion efficiency of PSCs. Thereby, a careful selection of ETL material and theoretical confirmation is essential to investigate for the PSCs. As far as HTL materials are concerned, Spiro-OMeTAD is widely used to produce the high efficiency PSCs [18–20]. Its good energy level alignment and decent conductivity after

* Corresponding author.
** Corresponding author.
*E-mail addresses:* kashif.riaz@itu.edu.pk (K. Riaz), zubairtarar@qu.edu.qa (Z. Ahmad).

https://doi.org/10.1016/j.optmat.2020.109897
Received 5 February 2020; Received in revised form 6 April 2020; Accepted 9 April 2020
Available online 18 April 2020

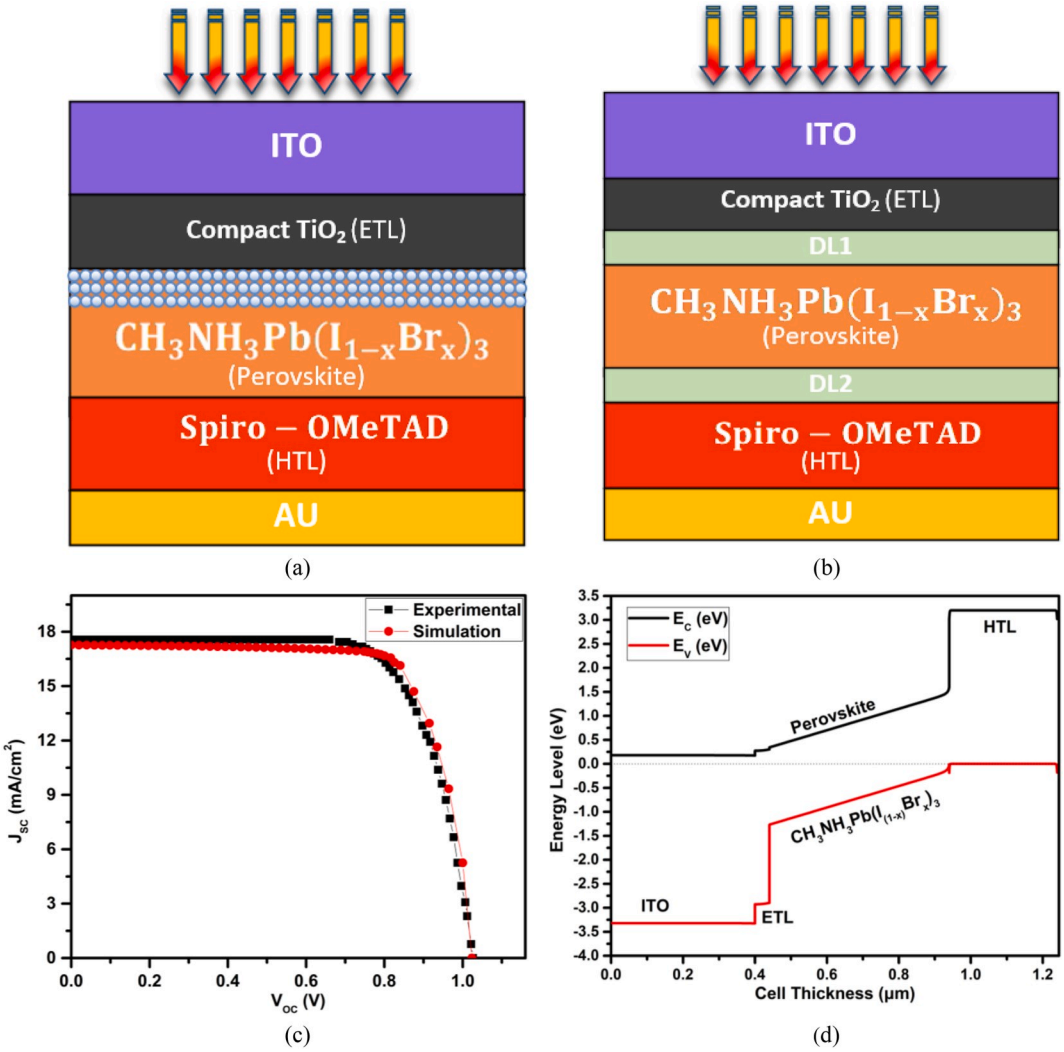


**Fig. 1.** (a) The schematic of the experimentally fabricated n-i-p structured PSCs (b) Schematic of the structure constructed for the simulation (using SCAPS-1D) with interface defect layers (DL1 and DL2). (c) numerically reproduced J-V characteristics of the experimentally fabricated n-i-p structured PSCs, (d) Energy band diagram of simulated PSCs.

doping [21] play a key role in the regeneration of perovskite absorber as well as extraction and transportation of photogenerated charge carriers to their respective electrode [22,23].

In this study, the SCAPS-1D simulator [24] has been used to numerically simulate the effects of various ETLs, while Spiro-OMeTAD was used as an HTL. First, we numerically reproduced the results (SCAPS-1D) for the experimentally designed stable perovskite solar cells based on ITO/$TiO_2$/$CH_3NH_3Pb(I_{1-x}Br_x)_3$/Spiro-OMeTAD/Au, and then the optimization of PSCs was done with respect to the doping concentrations of ETL and HTL layers. Henceforth, the optimized design of the PSCs (with respect to the doping concentrations) is further analyzed for the perovskite absorber layer thickness. Also, we investigated the effect of different ETL materials to find a promising replacement for $TiO_2$. Furthermore, the thickness of ETLs was varied to look at its impact on solar cell performance. Finally, a comparative analysis based on different ETL materials is performed to find the optimized PSC design.

Here it is important to note that SCAPS is a Windows-oriented program, which has been developed with LabWindows/CVI of National Instruments. The carrier densities, band graphs, current densities at any certain bias point can be calculated. The J-V simulation, recombination current, interface traps density, and quantum efficiency simulation can be performed. The working point in SCAPS can be specified by the parameters which are relevant to that measurement, such as illumination conditions, the initial working point, shunt conductance, and series resistance, recombination mechanisms, and SRH-types, etc. Previously, a comparative study of $TiO_2$ and ZnO-based electron transport layers were undertaken for $MAPbI_3$ based PSCs using SCAPS simulation by K. Adhikari et al. [25], in which the effect of absorber thickness was studied. In another work [26], the performance of $MAPbI_3$ perovskite absorber has been evaluated for different ETL and HTL materials, where the effect of defect density on PSC performance was investigated. Similarly, comparison for different ETLs by considering copper iodide as HTL was also performed using SCAPS for the $MAPbI_3$ based PSCs [27]. In addition to an absorber, HTL, and ETL layer thickness and defect density, several other parameters critically influence the PSC performance. These parameters include the doping concentrations of ETL and HTL, diffusion lengths, and CBO of ETL [28]. For example, a suitable CBO of ETL with the perovskite absorber can reduce the interface recombination [29]. Thus, a detailed and comprehensive investigation of all the parameters mentioned above is needed to understand the factors influencing the performance of the PSCs profoundly.

## 2. Device modeling and simulation

The schematic of the experimentally fabricated n-i-p structured using mixed perovskite precursor is shown in Fig. 1(a). Indium tin oxide (ITO)

**Table 1**
Input Parameters for PSC device simulation.

| Parameters | ITO | ETL | Defect layer, DL1 | Absorber $CH_3NH_3Pb(I_{1-x}Br_x)_3$ | Defect layer,DL2 | HTL (Spiro -OMeTAD) |
|---|---|---|---|---|---|---|
| Thickness (nm) | 500 | 40 | 10 [30] | 600 | 10 [30] | 300 |
| $E_g(eV)$ | 3.5 [27] | 3.2 [30] | 1.61 | 1.61 [32] | 1.61 | 3.0 [30] |
| $\chi(eV)$ | 4.0 [27] | Table S1 | 3.86 | 3.86 [33] | 3.86 | 2.45 [30] |
| $\varepsilon_r$ | 9 [30] | Table S1 | 6.5 | 6.5 [29] | 6.5 | 3 [30] |
| $N_c(cm^{-3})$ | $2.2x10^{+18}$ | $2.2x10^{+18}$ [30] | $2.2x10^{+18}$ | $2.2x10^{+18}$ [30] | $2.2x10^{+18}$ | $2.2x10^{+18}$ [30] |
| $N_v(cm^{-3})$ | $1.8x10^{+19}$ | $1.8x10^{+19}$ [30] | $1.8x10^{+19}$ | $1.8x10^{+19}$ [30] | $1.8x10^{+19}$ | $1.8x10^{+19}$ [30] |
| $\mu_n/(cm^{-3}/Vs)$ | 20 [27] | Table S1 | 2 | 2 [29] | 2 | 2E-4 [30] |
| $\mu_p/(cm^{-3}/Vs)$ | 10 [27] | Table S1 | 2 | 2 [29] | 2 | 2E-4 [30] |
| $N_D(cm^{-3})$ | $1x10^{+18}$ [30] | $1x10^{+21}$ | $1x10^{+13}$ | $1x10^{+13}$ [29] | $1x10^{+13}$ | 0 |
| $N_A(cm^{-3})$ | 0 | 0 | $1x10^{+13}$ | $1x10^{+13}$ [29] | $1x10^{+13}$ | $1x10^{+20}$ |
| $N_t(cm^{-3})$ | $1x10^{+15}$ [33] | $1x10^{+15}$ [29] | $1x10^{+17}$ [30] | $2.5x10^{+13}$ [31] | $1x10^{+17}$ [30] | $1x10^{+15}$ [30] |

$E_g$: Energy band gap; $\chi$:Electron Affinity; $\mathcal{E}_r$: Relative Permittivity; $N_c$: Conduction Band Density of States; $N_v$: Valance Band Density of states; $\mu_n$: Electron Mobility; $\mu_p$: Hole Mobility; $N_D$: Donor concentration; $N_A$: Acceptor Concentration; $N_t$: Defect Density.

is a transparent conducting oxide layer that acted as front contact in fabricated PSC. A mixed metal halide perovskite ($CH_3NH_3Pb(I_{1-x}Br_x)_3$) layer is sandwiched between compact-$TiO_2$/mesoporous-$TiO_2$ and Spiro-OMeTAD. $TiO_2$ and Spiro-OMeTAD acted as ETL and HTL layers, respectively, in $CH_3NH_3Pb(I_{1-x}Br_x)_3$ based PSC. Gold (Au) layer served as back metal contact in the PSC. A 1-D device simulation tool SCAPS

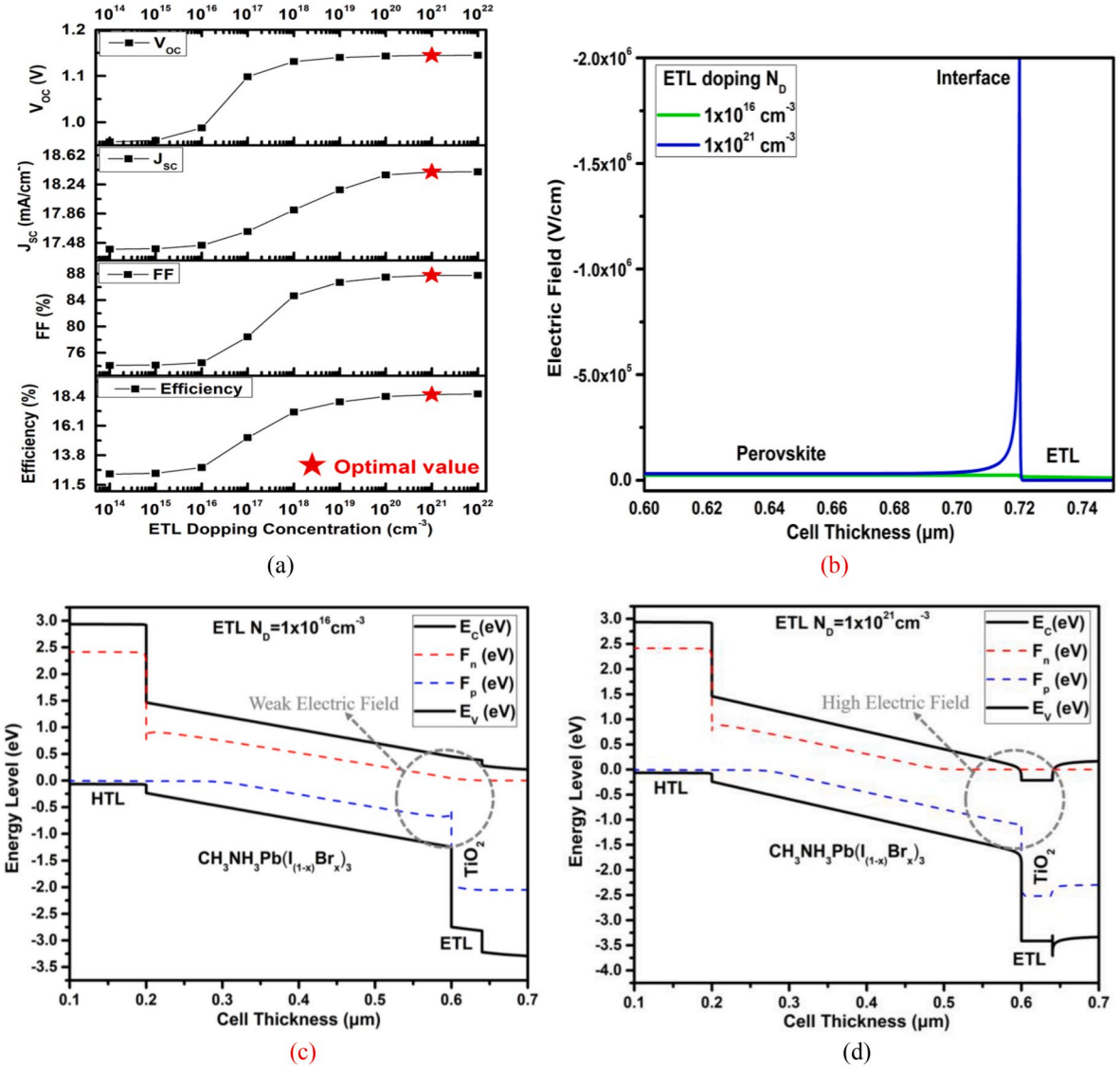


**Fig. 2.** (a) Effect of doping of ETL ($TiO_2$) on the photovoltaic parameters of PSCs, (b) Built-in electric field at the ETL/perovskite interface (c) Quasi-Fermi level separation under low doping concentration and (d) Quasi-Fermi level separation under high doping concentration.

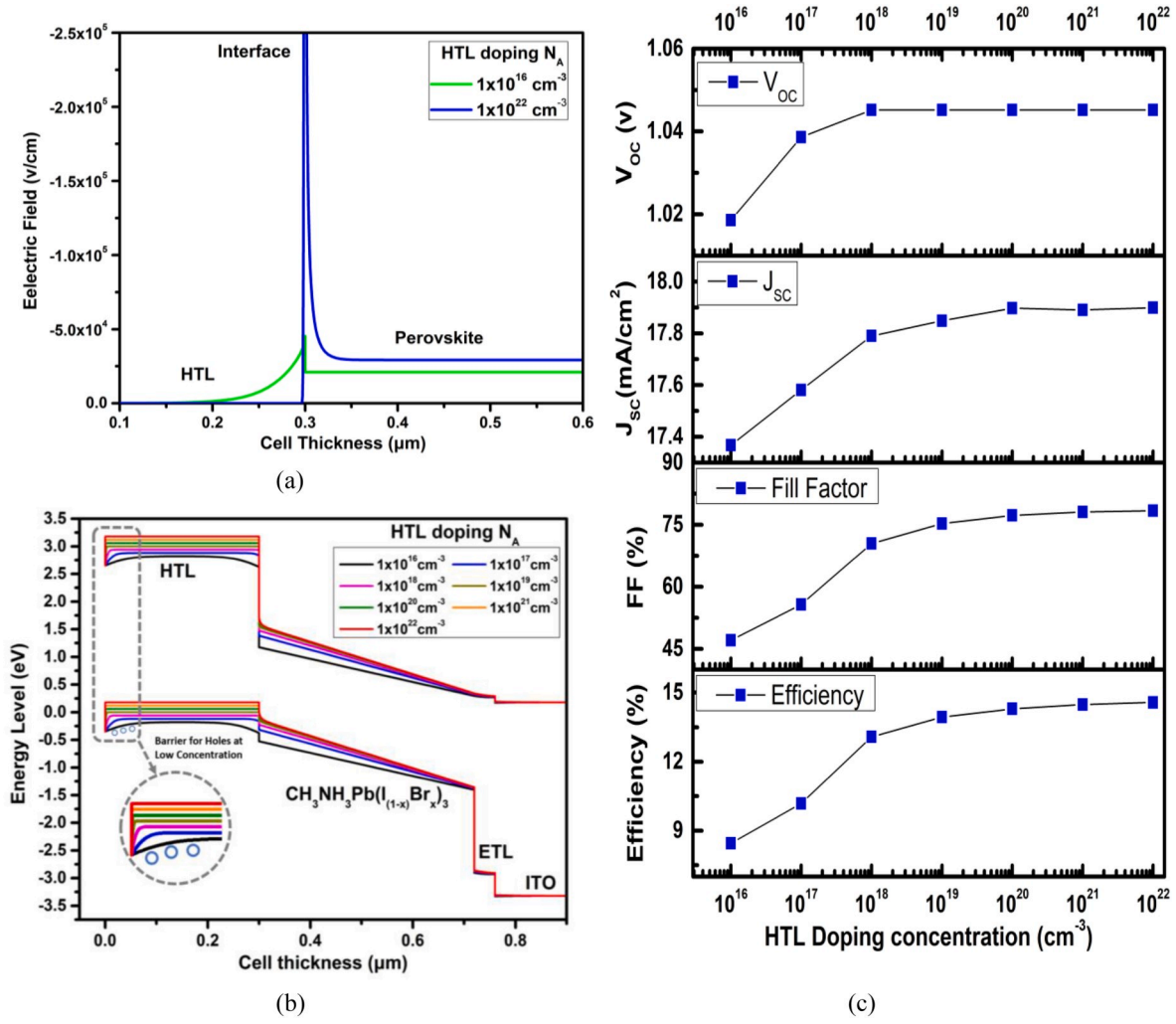


**Fig. 3.** (a) Effect of HTL doping on HTL/perovskite interface electric field (b) Effect of HTL doping on the Energy band diagram for (c) Effect of HTL doping on the photovoltaic parameters.

(ver. 3.305) based on Poisson and continuity equations is used [24] to model and simulate the PSC structure. The simulated structure of the PSC is constructed according to the experimentally designed PSCs (see Fig. 1(b). The interface defect layers (DL1 and DL2) were used between ETL/absorber interface and absorber/HTL interface in the simulated model to take into account the effect of carrier recombination at the layer interfaces [29]. Here it is important to note that for the inclusion mesoporous $TiO_2$ layer in the simulation, a 3D model is required. However, due to the limitation of the SCAP-1D, it has been considered as a part of the ETL as described in Ref. [30]. For the initial guessing and numerical model validation, the photovoltaic data of a very stable (over one year with PCE ~13%) n-i-p structured (ITO/$TiO_2$/$CH_3NH_3Pb(I_{1-x}Br_x)_3$/Spiro-OMeTAD/Au) was used. In this work, the ETL ($TiO_2$) was doped with LiTFSI while the HTL (spiro-OMeTAD) was doped with Li-TFSI and Co[t-BuPyPz]$_3$[TFSI]$_3$ (FK209) [31]. During the simulation, after reproducing the experimental results and I–V curve fitting in SCAPS, we kept all the parameters of base PSC constant. We varied the doping concentration of the ETL layer from $10^{14}$ $cm^{-3}$ to $10^{22}$ $cm^{-3}$. SCAPS provides both types of doping; graded, and uniform. Here, we used uniform doping both for ETL and HTL.

Table 1 summarizes the parameters and their values used in PSC simulations for each layer. Most of the parameter values are extracted from fabricated PSC devices and rest from the literature. Here $E_g$ is bandgap, $\chi$ is electron affinity, $\varepsilon_r$ is relative permittivity, $\mu_n$ and $\mu_p$ are electron and hole mobility, $N_A$ and $N_D$ are acceptor and donor concentrations, and $N_t$ is the defect density. Here, $N_t = 2.5x10^{13}$ $cm^{-3}$ for perovskite absorber in order to have the carrier diffusion lengths of 1 μm [32]. Conduction and valance bands' densities of states are taken to be $2.2x10^{18}$ $cm^{-3}$ and $1.8x10^{19}$ $cm^{-3}$ [29]. The Center of the bandgap is set for defect energy level and distributed in Gaussian, having an appropriate energy level to be 0.1eV [29]. For getting absorption coefficient $\alpha = A(hc\text{-}E_g)^{0.5}$ for perovskite, pre-factor $A$ is taken $1x10^5$ $cm^{-1}eV^{-0.5}$ [30]. The thermal velocities of electrons and holes are taken as $1x10^7$ $cms^{-1}$ [29]. The bandgap of the perovskite absorber $CH_3NH_3Pb(I_{1-x}Br_x)_3$ can be varied with bromide (Br) content [33]. Therefore, in this simulation, the bandgap of perovskite is expressed according to the literature [16]. The electron affinity of perovskite was set according to $\chi(x)=(3.9\text{-}0.55x)$ [34]. For numerically reproducing the experimental J-V characteristics of the fabricated PSCs, the simulation was performed according to fabricated structure, and their associated parameter values are given in Table 1. Fig. 1 (c) displays the experimental and numerically reproduced J-V characteristics of the experimentally designed PSCs. The energy band diagram of the simulated device under 0 V bias is shown in Fig. 1(d), here $E_C$ and $E_V$ are denoting the conduction band minimum and valance band minimum, respectively.

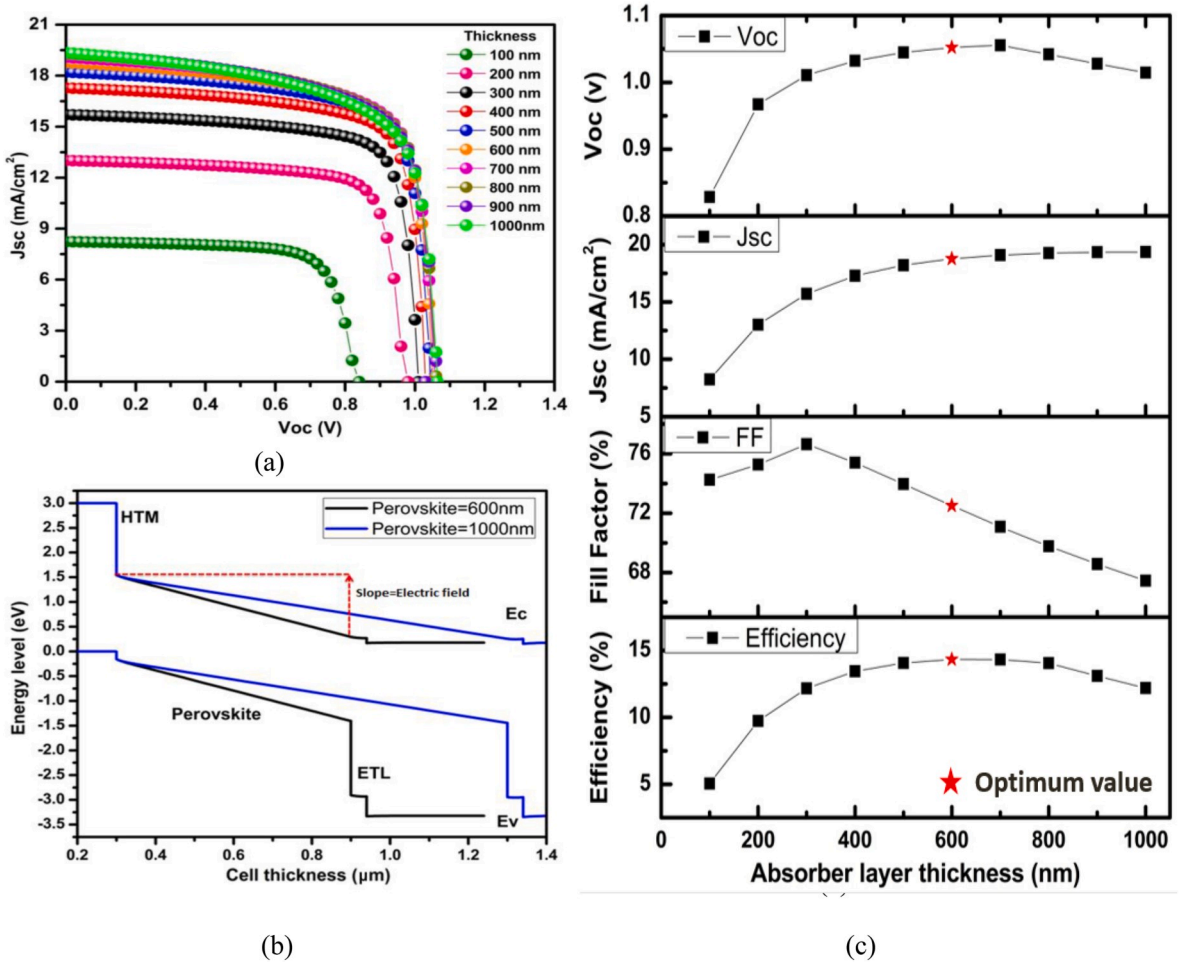


**Fig. 4.** (a) J-V characteristics for different Absorber layer thickness. (b) Effect of absorber layer thickness on the built-in electric field and (c) Effect of absorber layer thickness on the photovoltaic parameters.

## 3. Results and discussion

### 3.1. Effect of doping concentrations of ETL and HTL

ETL and HTL play a central role in the collection of generated charge carriers in PSCs. When light falls on the perovskite absorber, excitons (adjacent electron hole pairs) are produced [35]. These excitons have low binding energy and high diffusion lengths [35]. Therefore, they reach the ETL/perovskite interface and are dissociated due to the space charge layer (SCL) electric field at the interface. Consequently, electrons are transported to ETL, and holes transportation is blocked, simultaneously. Similarly, at the HTL/perovskite interface, holes are transported to the HTL layer due to the electric field, and electrons are correspondingly blocked due to barrier formation. These separated charge carriers move towards the respective electrodes and go into the external circuit through the metal contacts. Fig. 2 (a) shows the effect of ETL doping concentrations on the photovoltaic performance of the PSCs. Open-circuit voltage ($V_{oc}$), short-circuit current density ($J_{sc}$), fill factor (FF), and PCE ($\eta$) improve with an increasing doping concentration of the ETL layer. The doping concentration of each layer is varied from $10^{17}$ cm$^{-3}$ to $10^{22}$ cm$^{-3}$. High doping concentrations of ETL cause high electron conductivity and provide low resistance to the flow of electrons that are swept away from the perovskite absorber layer due to the presence of a strong built-in electric field as shown in Fig. 2 (b). A steep increase in the open-circuit voltage in Fig. 2(a) is due to the increased separation of the Quasi Fermi levels in non-equilibrium conditions. As depicted in Fig. 2(c) and (d), for low doping value of ETL Quasi Fermi levels are closer, whereas, for a high amount of doping, they are more separated from each other. A high doping concentration of ETL produces deep energy levels at the heterojunction interfaces that reduce the non-radiative recombination at the interface and improves the cell performance [36]. At high doping concentration, a strong electric field is produced, which effectively collects the electrons and strongly repels the minority carriers away from the ETL/perovskite interface, thus reducing interface recombination [36]. From Fig. 2 (a), it is evident that the values of all the parameters tend to saturate at higher doping concentrations. Therefore, an ETL concentration of $10^{21}$ cm$^{-3}$ would be an optimum value.

Similarly, high doping of HTL produces a strong electric field at the HTL/perovskite interface that blocks the flow of minority electrons towards the interface, thus reducing the interface recombination, as shown in Fig. 3 (a). A higher doping concentration of HTL moves the Fermi level of HTL towards the valence band, thus forming an ohmic contact with the back-metal electrode (Au) that subsequently leads to an efficient collection of holes at the contact [34]. At low doping concentration of HTL, a barrier is formed against the holes at the metal-semiconductor contact that causes their combination loss. This is explained via the energy band diagram shown in Fig. 3 (b). The same effect was also observed in the literature where it was established that the decreased work function of a contact layer systematically leads to an increasing Schottky barrier against the holes at the top interface of solar cells [37–39]. As illustrated in Fig. 3 (c), $J_{sc}$, $V_{oc}$, and Fill Factor (FF) are increasing with a corresponding increase in the HTL doping concentration. This improvement is saturated after a specific value of doping;

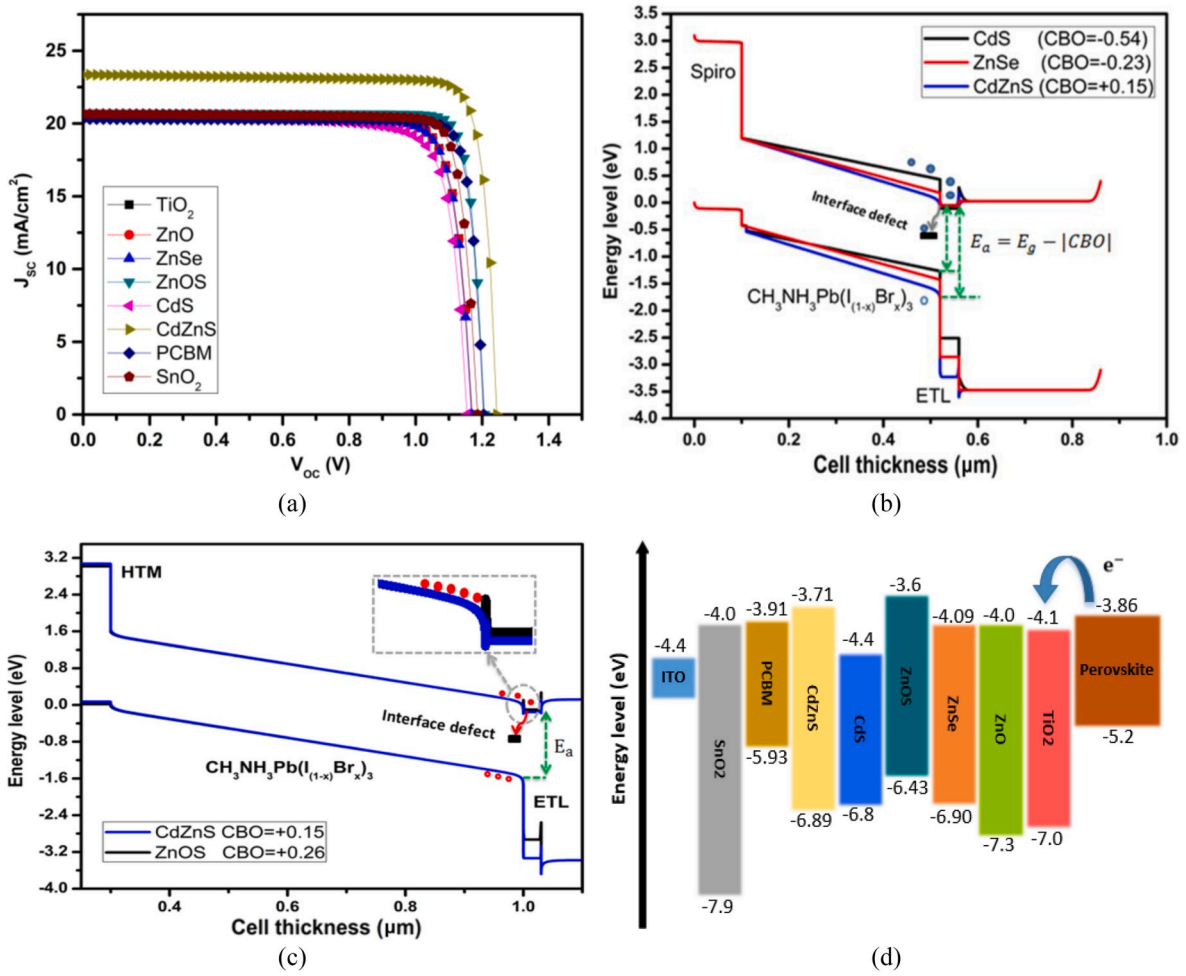


**Fig. 5.** (a) J-V characteristics of the simulated PSCs using different ETL materials, (b) Effect of CBO on the PSC performance, due to interface recombination (c) Comparison of ZnOS and CdZnS for + CBO (d) Energy band diagram for different ETL materials investigated in this study.

therefore, the feasible value for HTL doping concentration is found to be $10^{20}$ $cm^{-3}$.

### 3.2. Effect of perovskite absorber layer thickness

As evident from Fig. 4 (a) (perovskite absorber layer studied by varying it from 100 nm to 1000 nm), it can be noticed that a thin absorber layer is not beneficial for a solar cell as poor light absorption entails lower $J_{sc}$ and $\eta$ values. Similarly, a thicker absorber is also not suitable as it introduces a more significant route to transfer the photo-generated charge carriers that lead to high recombination. Therefore, optimum perovskite absorber thickness selection is necessary for an efficient PSC. Fig. 4 (b) illustrates the effect of absorber layer thickness on the built-in electric field using the 600 nm and 1000 nm perovskite absorber layer thickness. As compared to the 600 nm, the 1 μm thick perovskite layer produces a weaker electric field, which reduces the charge separation ability of the PSC and causes increased charge recombination. Fig. 4 (c) depicts the effect of absorber layer thickness on the photovoltaic parameters. The $J_{sc}$ is rising rapidly with increased absorber thickness. The reason for $J_{sc}$ rise is the increased rate of generation of charge carriers. $V_{oc}$ initially shows an increment; however, after a certain point, it saturates and tends to a slight decrease. FF of the device is continuously decreasing with the increasing thickness that could be associated with the reduced shunt resistance and increased series resistance (as depicted from the J-V characteristics presented in Fig. 4 (a)). PCE of PSC shows a steady rise until 600 nm thick absorber layer, even though it starts decreasing afterward. Here it is important to note that with the increase in the thickness of the absorber layer, the rates of both carrier generation and recombination rise (as shown in Fig. S1). Using the SCAPS-1D simulation, a 600 nm thick absorber layer is optimum for an efficient PSC using the $CH_3NH_3Pb(I_{1-x}Br_x)_3$ perovskite precursor.

**Table 2**
Output performance parameters of PSC due to different ETL materials.

| ETL Materials | $V_{oc}$ (V) | $J_{sc}$ ($mA/cm^2$) | FF (%) | η (%) |
|---|---|---|---|---|
| $TiO_2$ | 1.1696 | 20.6580 | 83.15 | 20.09 |
| ZnO | 1.1695 | 20.6530 | 83.12 | 20.90 |
| ZnSe | 1.1681 | 20.6173 | 82.76 | 19.93 |
| ZnOS | 1.2061 | 20.7057 | 88.28 | 22.05 |
| CdS | 1.1546 | 20.5167 | 80.87 | 19.16 |
| CdZnS | 1.2436 | 23.3594 | 86.29 | 25.20 |
| PCBM | 1.2043 | 20.3143 | 87.93 | 21.51 |
| SnO2 | 1.1861 | 20.6541 | 86.56 | 21.21 |

### 3.3. Effect of different ETL materials on PSC performance

In order to evaluate the performance of $CH_3NH_3Pb(I_{1-x}Br_x)_3$) based PSC, different ETL materials have also been considered. Materials such as Zinc oxide (ZnO), Zinc selenium (ZnSe), Zinc oxysulfide (ZnOS), cadmium sulfide (CdS), cadmium zinc sulfide (CdZnS), phenyl butyric acid methyl ester (PCBM), and tin dioxide ($SnO_2$) were studied and the results were compared with $TiO_2$ based ETL. The selection of these

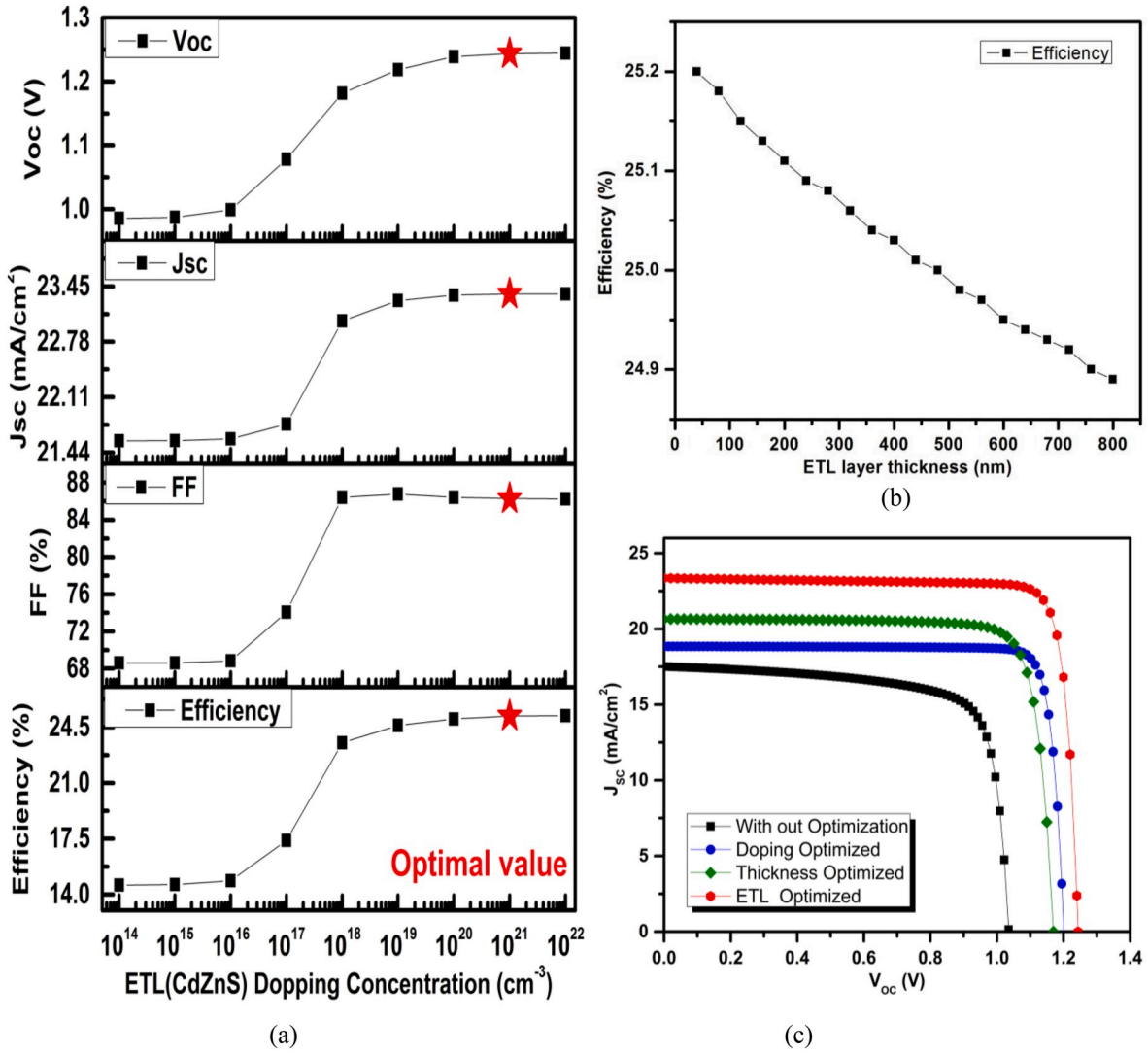


**Fig. 6.** (a) Effect of variation of ETL (CdZnS) doping concentration on photovoltaic parameters (b) Effect of variation of ETL (CdZnS) layer thickness from 40 nm to 800 nm (b)J-V characteristics of the optimized doping of ETL ($1x10^{21}$ $cm^{-3}$) and HTL ($1x10^{20}$ $cm^{-3}$), absorber thickness (600 nm) and ETM (CdZnS) based n-i-p perovskite solar cell.

materials for the ETL was made based on the previous reports on these materials. Fig. 5 (a) shows the J-V characteristics for each ETL material, and their simulation parameters are given in Table S1 taken from literature. The parameters of $TiO_2$, ZnO, ZnSe, and ZnOS were taken from Ref. [27,30,40], whereas the parameters for CdZnS, CdS, PCBM and $SnO_2$ are adopted from references [26,41–44]. The corresponding key performance factors for each ETL are summarized in Table 2. The results demonstrate that CdZnS offers higher efficiency as compared to the others investigated ETL materials. These results can be explained with reference to the conduction band offset between ETL/perovskite absorber interface and bandgap alignment. The energy level diagram of different ETL materials is shown in Fig. 5 (d). Here the conduction band offset (CBO) is defined as the difference of electron affinities of ETL and perovskite absorber (CBO = $\chi_{perovskite} - \chi_{ETL}$) [45]. An energy band diagram representation of CBO for ETL is given in Fig. S2. If CBO between the ETL/absorber interface is negative, then there is a cliff formed at the interface that supports the flow of electrons from perovskite to ETL due to the high electric field at the interface and results in high $J_{sc}$ [29,43]. However, the higher negative value decreases the activation energy ($E_a$) for recombination at the ETL/perovskite interface; therefore, it reduces $V_{oc}$ and hence the performance of the cell. CBO of different ETLs given in Table S2. In the case of CdZnS, $J_{sc}$ and $V_{oc}$ value are the highest among all ETL investigated materials, which may be due to its + CBO of 0.15 and higher carrier mobility. It has large activation energy ($E_a$) of recombination at the interface. In the case of CdS, the CBO is −0.54 that results in a cliff formation at the absorber/ETL interface, and the $E_a$ is smallest among all the investigated ETL materials, as illustrated in Fig. 5 (b). Due to this large cliff formation and smaller $E_a$, it produces low $V_{oc}$ and PCE. PCBM has smallest negative CBO of −0.05 but due to low carrier mobilities of ($2x10^{-1}$ $cm^{-2}$/V) it gives low $J_{sc}$ and efficiency than CdZnS.

As CBO gets more negative, the activation energy ($E_a = E_g$ - |CBO|) of recombination lowers, which increases the probability of recombination of transferring electrons at the absorber/ETL interface. This results in reducing the $V_{oc}$ due to substantial interface recombination. Whereas, in the case of +CBO, $E_a$ gets large, which reduces the interface recombination and improves the $V_{oc}$ and PCE. CdZnS gives the highest $J_{sc}$, $V_{oc}$, and efficiency due to + CBO. However, as CBO gets more positive, it introduces a small spike at the ETL/absorber interface, which reduces the cell efficiency a bit due to barrier in the path of transferring electrons as it has been observed in the case of ZnOS (with CBO of +0.26). As depicted in Fig. 5 (c), the value of activation energy for ZnOS and CdZnS is high and close to each other due to which they have low interface recombination and resultantly high $V_{oc}$ and PCE. Though ZnOS has a

greater value of +CBO as compare to CdZnS, it has less PCE due to the formation of the spike at the absorber/ETL interface, which hinders the flow of electrons. Thereby large values of +CBO are also not suitable for charge transportation in PSCs.

The effect of the doping concentration of CdZnS was also evaluated on the performance of the optimized PSCs. As illustrated in Fig. 6 (a), $J_{sc}$, $V_{oc}$, and FF are increasing with a corresponding increase in the CdZnS doping concentration. This improvement is saturated after a specific value of $10^{21}$ $cm^{-3}$; therefore, the feasible value for CdZnS doping concentration is found to be $10^{21}$ $cm^{-3}$. Furthermore, the thickness of CdZnS was also varied to see its effect on cell performance. It was observed from the simulation that as the thickness of CdZnS was increased from 40 nm to 800 nm, the cell efficiency had started dropping, as shown in Fig. 6 (b). This might be due to increased light absorption in the ETL layer, which causes fewer photons to reach to actual perovskite absorber layer [43]. It might also be due to increased series resistance of the PSC due to increased ETL thickness, thereby 40 nm is the optimal value for CdZnS. In Fig. 6 (c), the final optimized planar perovskite solar cell J-V characteristics are shown. Here, the baseline fabricated PSC device was optimized through step by step process of doping concentration of ETL and HTL, absorber layer thickness, and ETL materials optimization. A comparison of results is also given in Table S3.

## 4. Conclusion

In summary, the perovskite solar cell structure ITO/ETL/$CH_3NH_3Pb(I_{1-x}Br_x)_3$/Spiro-OMeTAD/Au has been numerically simulated using SCAPS-1D software. It has been observed that the PSC performance is profoundly affected by the doping concentrations of ETL and HTL. By increased doping of these charge transport layers (CTLs), $V_{oc}$ and PCE of the PSC improve due to, more energetic built in the field, increased conductivity and quasi fermi levels separation. The optimal thickness for mixed halide perovskite absorber has been obtained to be 600 nm. It has been found that CBO between the ETL/absorber interface plays a crucial role in cell performance. When the CBO has a negative value, then the activation energy ($E_a$) of interface recombination becomes small; as a result, $V_{oc}$ and cell efficiency decreases. However, positive CBO has a large activation energy of interface recombination; thus, it gives large values of $V_{oc}$ and better cell performance. In the comparative study of different ETLs based on CBO, CdZnS has produced the highest $J_{sc}$ (23.3594 $mA/cm^{-2}$), $V_{oc}$ (1.2436 v), and efficiency (25.20%). This numerical work implies that proper energy level alignment of ETL, CBO, doping of CTLs, and absorber thickness are a primary requirement to achieve the high efficiency of the PSCs. This work could be helpful for the design and optimization of Br–I based mixed halide perovskite solar cells.

## Authors contribution

All authors contributed equally.

## Data availability statement

The data that support the findings of this study are available from the corresponding author upon reasonable request.

## Declaration of competing interest

The authors declare that they have no known competing financial interests or personal relationships that could have appeared to influence the work reported in this paper.

## Acknowledgment

This publication was made possible by the NPRP award [NPRP11S-1210–170080] from Qatar National Research Fund (a member of the Qatar Foundation). The findings made herein are solely the responsibility of the authors. The authors are thankful to Prof. Marc Burgelman, the University of Gent for the SCAPS developments package, and permission to use the SCAPS software.

## Appendix A. Supplementary data

Supplementary data to this article can be found online at https://doi.org/10.1016/j.optmat.2020.109897.

## References

[1] J. Chen, N.G. Park, Causes and Solutions of Recombination in Perovskite Solar Cells, Advanced Materials, 2018, p. 1803019.
[2] T.W. Jones, A. Osherov, M. Alsari, M. Sponseller, B.C. Duck, Y.-K. Jung, C. Settens, F. Niroui, R. Brenes, C.V. Stan, Lattice strain causes non-radiative losses in halide perovskites, Energy Environ. Sci. 12 (2019) 596–606.
[3] D. Luo, R. Su, W. Zhang, Q. Gong, R. Zhu, Minimizing non-radiative recombination losses in perovskite solar cells, Nature Reviews Materials (2019), https://doi.org/10.1038/s41578-019-0151-y.
[4] N.E. Courtier, J.M. Cave, J.M. Foster, A.B. Walker, G. Richardson, How transport layer properties affect perovskite solar cell performance: insights from a coupled charge transport/ion migration model, Energy Environ. Sci. 12 (2019) 396–409.
[5] S. Pisoni, M. Stolterfoht, J. Löckinger, T. Moser, Y. Jiang, P. Caprioglio, D. Neher, S. Buecheler, A.N. Tiwari, On the Origin of Open-Circuit Voltage Losses in Flexible Nip Perovskite Solar Cells, Science and Technology of Advanced Materials, 2019.
[6] S. Ravishankar, S. Gharibzadeh, C. Roldán-Carmona, G. Grancini, Y. Lee, M. Ralaiarisoa, A.M. Asiri, N. Koch, J. Bisquert, M.K. Nazeeruddin, Influence of charge transport layers on open-circuit voltage and hysteresis in perovskite solar cells, Joule 2 (2018) 788–798.
[7] M. Stolterfoht, P. Caprioglio, C.M. Wolff, J.A. Márquez, J. Nordmann, S. Zhang, D. Rothhardt, U. Hörmann, Y. Amir, A. Redinger, The impact of energy alignment and interfacial recombination on the internal and external open-circuit voltage of perovskite solar cells, Energy Environ. Sci. 12 (2019) 2778–2788.
[8] K.K. Wong, A. Fakharuddin, P. Ehrenreich, T. Deckert, M. Abdi-Jalebi, R.H. Friend, L. Schmidt-Mende, Interface-dependent radiative and nonradiative recombination in perovskite solar cells, J. Phys. Chem. C 122 (2018) 10691–10698.
[9] Y. Wu, X. Yang, H. Chen, K. Zhang, C. Qin, J. Liu, W. Peng, A. Islam, E. Bi, F. Ye, Highly compact TiO2 layer for efficient hole-blocking in perovskite solar cells, APEX 7 (2014), 052301.
[10] A. Djurišić, F. Liu, H. Tam, M. Wong, A. Ng, C. Surya, W. Chen, Z. He, Perovskite solar cells-An overview of critical issues, Prog. Quant. Electron. 53 (2017) 1–37.
[11] J. Shi, J. Liang, S. Peng, W. Xu, J. Pei, J. Chen, Synthesis, characterization and electrochemical properties of a compact titanium dioxide layer, Solid State Sci. 11 (2009) 433–438.
[12] N.J. Jeon, J.H. Noh, W.S. Yang, Y.C. Kim, S. Ryu, J. Seo, S.I. Seok, Compositional engineering of perovskite materials for high-performance solar cells, Nature 517 (2015) 476.
[13] P. Tiwana, P. Docampo, M.B. Johnston, H.J. Snaith, L.M. Herz, Electron mobility and injection dynamics in mesoporous ZnO, SnO2, and TiO2 films used in dye-sensitized solar cells, ACS Nano 5 (2011) 5158–5166.
[14] D. Liu, S. Li, P. Zhang, Y. Wang, R. Zhang, H. Sarvari, F. Wang, J. Wu, Z. Wang, Z. D. Chen, Efficient planar heterojunction perovskite solar cells with Li-doped compact TiO2 layer, Nano Energy 31 (2017) 462–468.
[15] J. Wang, M. Qin, H. Tao, W. Ke, Z. Chen, J. Wan, P. Qin, L. Xiong, H. Lei, H. Yu, Performance enhancement of perovskite solar cells with Mg-doped TiO2 compact film as the hole-blocking layer, Appl. Phys. Lett. 106 (2015) 121104.
[16] J.M. Ball, M.M. Lee, A. Hey, H.J. Snaith, Low-temperature processed meso-superstructured to thin-film perovskite solar cells, Energy Environ. Sci. 6 (2013) 1739–1743.
[17] W. Ke, C.C. Stoumpos, J.L. Logsdon, M.R. Wasielewski, Y. Yan, G. Fang, M. G. Kanatzidis, TiO2–ZnS cascade electron transport layer for efficient formamidinium tin iodide perovskite solar cells, J. Am. Chem. Soc. 138 (2016) 14998–15003.
[18] N. Ahn, D.-Y. Son, I.-H. Jang, S.M. Kang, M. Choi, N.-G. Park, Highly reproducible perovskite solar cells with average efficiency of 18.3% and best efficiency of 19.7% fabricated via Lewis base adduct of lead (II) iodide, J. Am. Chem. Soc. 137 (2015) 8696–8699.
[19] D. Bi, W. Tress, M.I. Dar, P. Gao, J. Luo, C. Renevier, K. Schenk, A. Abate, F. Giordano, J.-P.C. Baena, Efficient luminescent solar cells based on tailored mixed-cation perovskites, Science advances 2 (2016), e1501170.
[20] X. Wang, J. Wu, Y. Yang, X. Liu, Q. Guo, Z. Song, G. Li, Z. Lan, M. Huang, High performance and stable perovskite solar cells using vanadic oxide as a dopant for spiro-OMeTAD, J. Mater. Chem. 7 (2019) 13256–13264.
[21] Z. Hawash, L.K. Ono, Y. Qi, Photovoltaics: recent advances in spiro-MeOTAD hole transport material and its applications in organic–inorganic halide perovskite solar cells (adv. Mater. Interfaces 1/2018, Advanced Materials Interfaces 5 (2018) 1870003.
[22] P. Docampo, S. Guldin, T. Leijtens, N.K. Noel, U. Steiner, H.J. Snaith, Lessons learned: from dye-sensitized solar cells to all-solid-state hybrid devices, Adv. Mater. 26 (2014) 4013–4030.

[23] Z. Yu, L. Sun, Recent progress on hole-transporting materials for emerging organometal halide perovskite solar cells, Advanced Energy Materials 5 (2015) 1500213.
[24] M. Burgelman, P. Nollet, S. Degrave, Modelling polycrystalline semiconductor solar cells, Thin Solid Films 361 (2000) 527–532.
[25] K.R. Adhikari, S. Gurung, B.K. Bhattarai, B.M. Soucase, Comparative study on MAPbI3 based solar cells using different electron transporting materials, Phys. Status Solidi 13 (2016) 13–17.
[26] F. Azri, A. Meftah, N. Sengouga, A. Meftah, Electron and hole transport layers optimization by numerical simulation of a perovskite solar cell, Sol. Energy 181 (2019) 372–378.
[27] M.M. Salah, K.M. Hassan, M. Abouelatta, A. Shaker, A comparative study of different ETMs in perovskite solar cell with inorganic copper iodide as HTM, Optik 178 (2019) 958–963.
[28] C. Momblona, L. Gil-Escrig, E. Bandiello, E.M. Hutter, M. Sessolo, K. Lederer, J. Blochwitz-Nimoth, H.J. Bolink, Efficient vacuum deposited pin and nip perovskite solar cells employing doped charge transport layers, Energy Environ. Sci. 9 (2016) 3456–3463.
[29] T. Minemoto, M. Murata, Theoretical analysis on effect of band offsets in perovskite solar cells, Sol. Energy Mater. Sol. Cell. 133 (2015) 8–14.
[30] T. Minemoto, M. Murata, Device modeling of perovskite solar cells based on structural similarity with thin film inorganic semiconductor solar cells, J. Appl. Phys. 116 (2014), 054505.
[31] Z. Ahmad, T. Noma, S. Paek, K.T. Cho, D. Taguchi, M. Iwamoto, T. Manaka, M. K. Nazeeruddin, F. Touati, S.A. Al-Muhtaseb, Stability in 3D and 2D/3D hybrid perovskite solar cells studied by EFISHG and IS techniques under light and heat soaking, Org. Electron. 66 (2019) 7–12.
[32] S.D. Stranks, G.E. Eperon, G. Grancini, C. Menelaou, M.J. Alcocer, T. Leijtens, L. M. Herz, A. Petrozza, H.J. Snaith, Electron-hole diffusion lengths exceeding 1 micrometer in an organometal trihalide perovskite absorber, Science 342 (2013) 341–344.
[33] Y. Zhou, F. Wang, H.-H. Fang, M.A. Loi, F.-Y. Xie, N. Zhao, C.-P. Wong, Distribution of bromine in mixed iodide–bromide organolead perovskites and its impact on photovoltaic performance, J. Mater. Chem. 4 (2016) 16191–16197.
[34] A. Rolland, L. Pedesseau, M. Kepenekian, C. Katan, Y. Huang, S. Wang, C. Cornet, O. Durand, J. Even, Computational analysis of hybrid perovskite on silicon 2-T tandem solar cells based on a Si tunnel junction, Opt. Quant. Electron. 50 (2018) 21.
[35] P. Lopez-Varo, J.A. Jiménez-Tejada, M. García-Rosell, S. Ravishankar, G. Garcia-Belmonte, J. Bisquert, O. Almora, Device physics of hybrid perovskite solar cells: theory and experiment, Advanced Energy Materials 8 (2018) 1702772.
[36] L. Xu, R. Molaei Imenabadi, W.G. Vandenberghe, J.W. Hsu, Minimizing performance degradation induced by interfacial recombination in perovskite solar cells through tailoring of the transport layer electronic properties, Apl. Mater. 6 (2018), 036104.
[37] H. Mehmood, T. Tauqeer, H. Nasser, S. Hussain, R. Turan, Effect of hole-selective molybdenum oxide work function and silicon wafer resistivity on dopant-free asymmetric silicon heterostructure solar cell, in: 2017 International Renewable and Sustainable Energy Conference (IRSEC), IEEE, 2017, pp. 1–5.
[38] H. Mehmood, H. Nasser, T. Tauqeer, S. Hussain, E. Ozkol, R. Turan, Simulation of an efficient silicon heterostructure solar cell concept featuring molybdenum oxide carrier-selective contact, Int. J. Energy Res. 42 (2018) 1563–1579.
[39] H. Mehmood, H. Nasser, T. Tauqeer, R. Turan, Simulation of silicon heterostructure solar cell featuring dopant-free carrier-selective molybdenum oxide and titanium oxide contacts, Renew. Energy 143 (2019) 359–367.
[40] S.I. Rahman, S. Faisal, S. Ahmed, T.I. Dhrubo, A Comparative Study on Different HTMs in Perovskite Solar Cell with ZnOS Electron Transport Layer, 2017 IEEE Region 10 Humanitarian Technology Conference (R10-HTC), IEEE, 2017, pp. 546–550.
[41] F. Baig, Y.H. Khattak, B. Marí, S. Beg, A. Ahmed, K. Khan, Efficiency enhancement of CH 3 NH 3 SnI 3 solar cells by device modeling, J. Electron. Mater. 47 (2018) 5275–5282.
[42] F. Baig, Y.H. Khattak, B. Marí, S. Beg, S.R. Gillani, A. Ahmed, Mitigation of interface recombination by careful selection of ETL for efficiency enhancement of MASnI3 solar cell, Optik 170 (2018) 463–474.
[43] T.H. Chowdhury, M.T. Ferdaous, M.A.A. Wadi, P. Chelvanathan, N. Amin, A. Islam, N. Kamaruddin, M.I.M. Zin, M.H. Ruslan, K.B. Sopian, Prospects of ternary Cd 1− x Zn x S as an electron transport layer and associated interface defects in a planar lead halide perovskite solar cell via numerical simulation, J. Electron. Mater. 47 (2018) 3051–3058.
[44] Y. Wang, Z. Xia, Y. Liu, H. Zhou, Simulation of perovskite solar cells with inorganic hole transporting materials, in: 2015 IEEE 42nd Photovoltaic Specialist Conference (PVSC), IEEE, 2015, pp. 1–4.
[45] C. Ding, Y. Zhang, F. Liu, Y. Kitabatake, S. Hayase, T. Toyoda, K. Yoshino, T. Minemoto, K. Katayama, Q. Shen, Effect of the conduction band offset on interfacial recombination behavior of the planar perovskite solar cells, Nano Energy 53 (2018) 17–26.